Hindawi
Geofluids
Volume 2021, Article ID 5557033, 13 pages
https://doi.org/10.1155/2021/5557033

WILEY | Hindawi

Research Article

Experimental Evaluation of Multiple Frost Heaving Parameters for Preflawed Granite in Beizhan Iron Mining, Xinjiang, China

Yu Wang, Dayu Long, Zulifeiya Rejuti, and Huajian Wang

Beijing Key Laboratory of Urban Underground Space Engineering, Department of Civil Engineering, School of Civil & Resource Engineering, University of Science & Technology Beijing, Beijing 100083, China

Correspondence should be addressed to Yu Wang; wyzhou@ustb.edu.cn

Received 6 January 2021; Revised 25 January 2021; Accepted 1 February 2021; Published 16 February 2021

Academic Editor: Feng Xiong

Ice-driven mechanical weathering in cold regions is considered a main factor impacting the stability of rock mass. In this work, the response surface method (RSM) was employed to evaluate and optimize the multiple frost heaving parameters to seek the maximum frost heaving force (FHF), in combination with experimental modeling based on a specially designed frost heaving force measurement system. Three kinds of rocks were prepared with parallel flaws in it having different flaw width, length, and cementation type, and these factors were used to fit an optimal response of the maximum FHF. The experimental results reveal five distinguished stages from the frost heaving force curve, and they are inoculation stage, explosive stage, decline to steady stage, recovery stage, and sudden drop stage. The sensitivity analysis reveals the influential order of the considered factors to peak FHF, which is the rock lithology, flaw width, flaw cement type, and flaw length. For low-porosity hard rock, increasing flaw width, flaw length, and flaw cement strength can improve the probability of frost heaving failure. It is suggested that rock lithology determines the water migration ability and influences the water-ice phase transformation a lot.

1. Introduction

Freeze-thaw (F-T) weathering frequently occurs in cold regions. Water from the thawing of snow or sleet penetrates into rock discontinuities (e.g., bedding planes, interbeds, cracks, foliation, flaw, and fault), and freeze occurs when the temperature is below zero. Under freezing conditions, 9% volume expansion occurs when water becomes ice [1–5], generating frost heave forces at preexisting cracks or discontinuities. The frost heave force drives the expansion of the geological discontinuities, which leads to the increase of the aperture and length of the fracture and the deterioration of the rock structure. The ice-driven mechanical weathering is generally considered a crucial process that impacts the long-term stability of rock mass. The rupture of rock bridge has been proved that it is triggered by ice-driven mechanical weathering [6, 7]. Therefore, it is crucial to investigate the evolution of frost heaving force in order to improve the understanding ability to ice-driven mechanical weathering in cold regions.

Nowadays, plenty of field, experimental, and theoretical studies have addressed the mechanics of frost wedging [8–10]; however, the temporal and spatial factors that control the frost heaving process remain elusive [1, 10–12]. Over the last few years, the volumetric expansion and ice segregation have been identified as two completing theory responsible for frost weathering [13]. The volumetric expansion theory argues that ice-induced expansion increases tensional stress at crack tip and leads to the increment of crack scale. In contrast, the ice segregation theory argued that water films exist among mineral interfaces; van der Waals and electrostatic forces apply disjoining pressure to separate ice from substrate [14, 15]. The ice segregation mechanism and associated disjoining forces are considered being able to fracture the rock. Commonly,

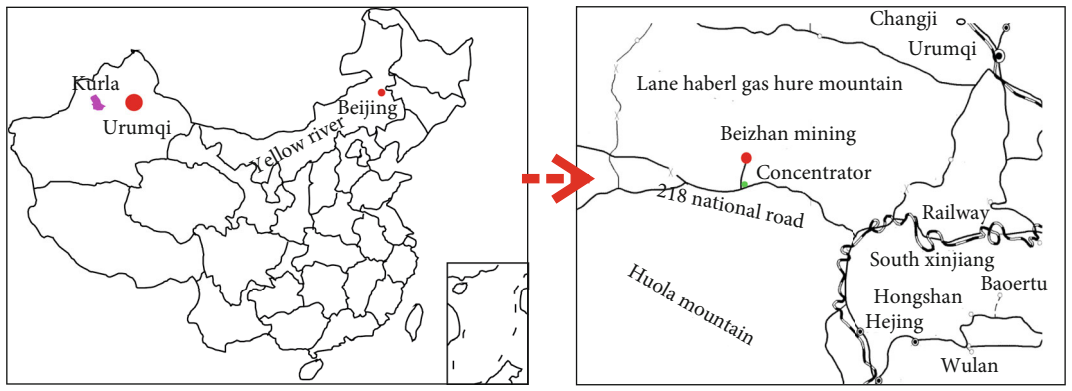

Figure 1: Description of the rock mass structural characteristics in the eastern open pit slope of Beizhan iron mine. Obvious rock bridge structure can be observed from the outcrop.

these two theories coexist and simultaneously lead to the fracture of rock. For low-porosity hard rock, the frost heaving force induced by the expansion of freezing water is believed to be the principal reason responsible for shattering jointed and low-permeability rocks in cold regions, as has been proved in many experiments [16–18]. The critical nucleus size for ice formation has been probed by Bai et al. [19]. They pointed out that frost force during water freezes is related to the size of nucleus. As the driving force to fracture solid objects, many experimental and theoretical investigations have been carried out to study the evolution of frost heaving force. Some scholars measured the frost heaving force by ice extrusion in open flaws, and it is from 0 to 7 MPa. This finding has also been proved from field investigation [17]. Winkler [18] pointed out that the frost heaving force by pore water freezing can reach to tens to hundreds MPa. Akagawa and Fukuda [20] proposed a theoretical equation to calculate the frost heaving force by segregation freezing theory. Arosio et al. [21] used thin film pressure sensor to test the frost heaving force of the preflawed rock samples after water filling, and the maximum frost heaving force was up to 5 MPa. Davidson et al. [22] measured the maximum frost heaving force of the saturated crack with a width of 1 mm in a transparent material by photoelastic test and found that the frost heaving force was 1.1 MPa. Huang et al. [23] preformed frost heaving measurement experiments in rock-like material by using a thin film pressure sensor, and the evolution process of frost heaving force was discussed.

As is known, frost heaving force is affected by many factors, such as geometry of the flaws [24, 25], rock saturation degree [26], thermodynamic parameters [27, 28], rock mechanical parameters [29, 30], and freezing direction [16]. Therefore, the relationship between frost heaving force and those parameters needs to be deeply studied in order to reveal the ice-driven mechanical weathering mechanism. After detailed literature review, it is found that studies about multiple factors influencing frost heaving force are not well understood. Especially, there are few reports about experimental investigation on frost heaving force evolution. As a result, the primary purpose of this study is to reveal the impact of flaw (cavity) geometric shape and rock physical properties on frost heaving force evolution. A response surface optimization algorithm is employed to evaluate multiple factors impacting the frost heaving force.

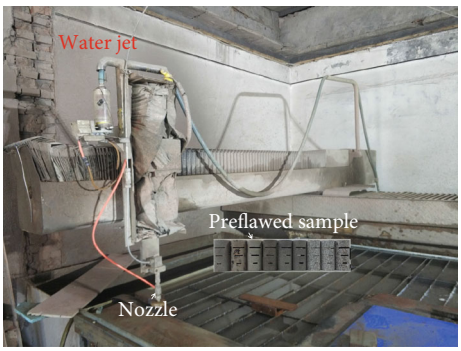

Figure 2: Production of the granite samples with two preexisting flaws for the fatigue mechanical test.

Figure 3: The vacuum saturation apparatus for the preflawed samples.

2. Frost Heaving Force Measurement

2.1. Rock Material Descriptions. The tested rock materials were obtained from a high-altitude alpine mining of the

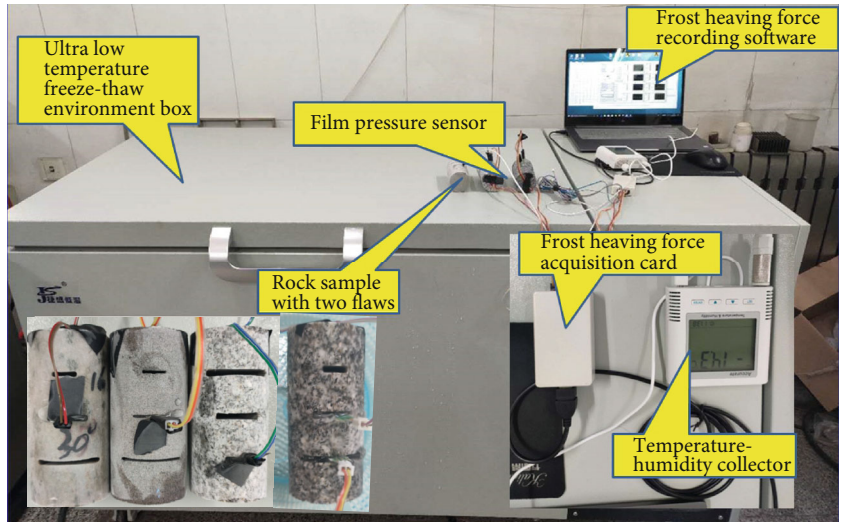

Figure 4: The frost heaving force measurement system developed in this work.

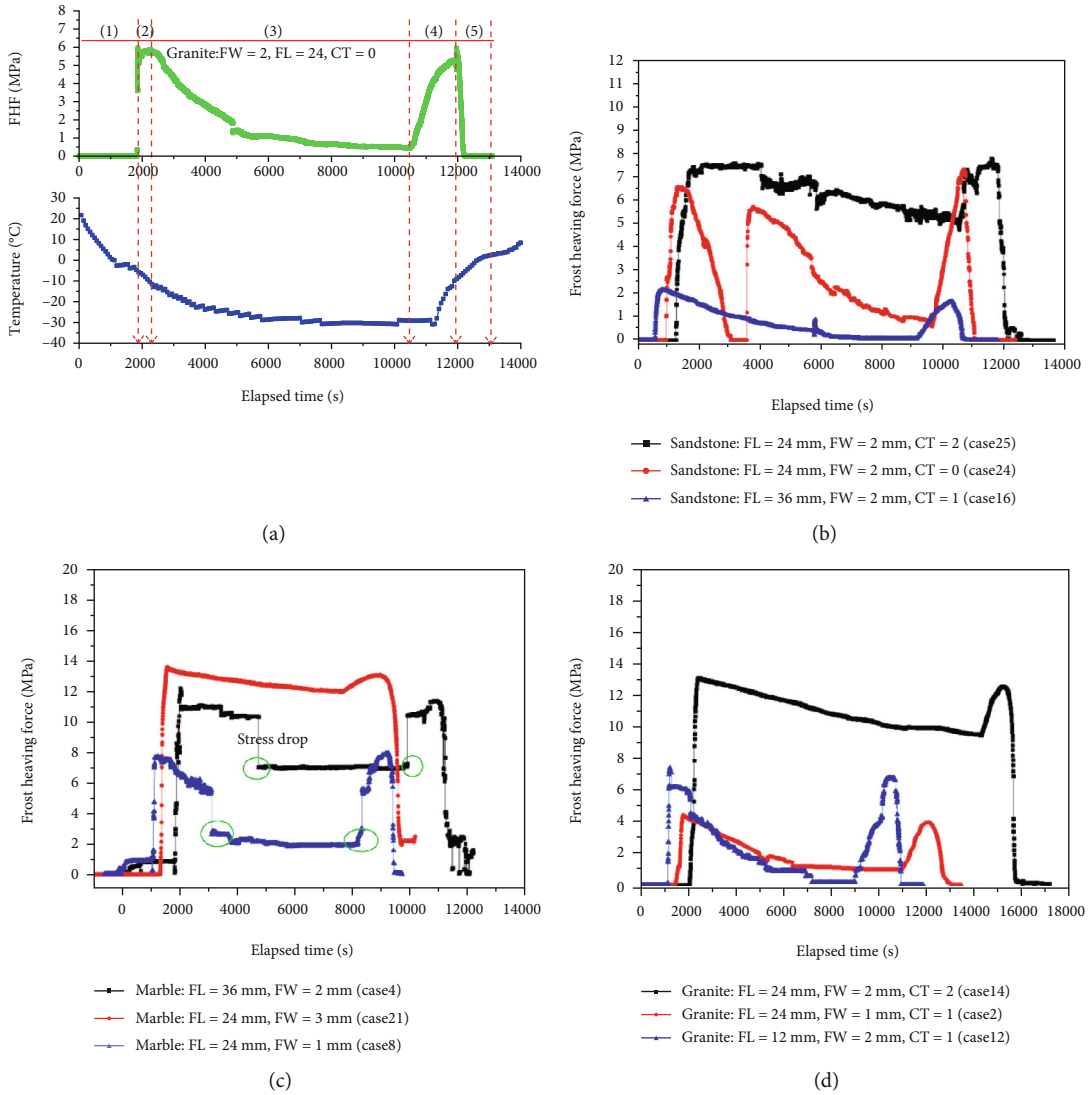

Figure 5: Evolution of frost heaving force for typical experimental cases. (a) Evolution stages division, taking case 6 for example. (b) Frost heaving force curves for typical marble samples. (d) Frost heaving force curves for typical granite samples.

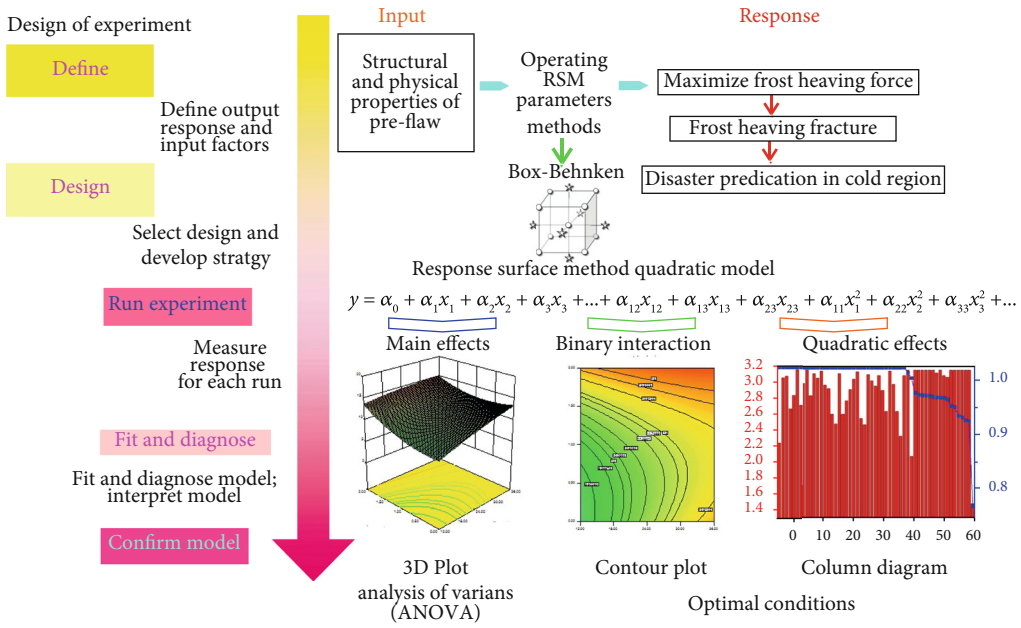

Figure 6: The solving steps of response surface method to maximum the frost heaving force.

Table 1: The considered factors influencing frost heaving force and their levels for the RSM model.

Influential factors	Coded symbol	Levels			Unit
		Minimum (-1)	Mean (0)	Maximum (+1)	
Width (FW)	A	1	2	3	mm
Length (FL)	B	12	24	36	mm
Cement type (CT)	C	0	1	2	/
Rock lithology (RL)	D	-1	0	1	/

Hejing Beizhan open pit slope in Xinjiang, northwest China (Figure 1(a)). The mining area is 123 kilometers away from Jingxiang County in the direction of 327°, and 84 kilometers away from Barongtai Town in Hejing County, as shown in Figure 1(a).The mine is located near the Tianshan Ridge on the north slope of Boluo Huoluo Mountain. The mountain is close to the east and west, and the overall terrain is high in the south and low in the north, with an elevation of 3160~4575 m and a relative elevation of 700~1000 m. The orebody is located at an altitude of 3450~3723 m. The mining area belongs to the continental temperate semiarid climate and is in the cold climate area, with mountain snow all year round and slope area snow from October to the next July (Figure 1(b)). The average temperature from January to April and from September to December is below zero, with the lowest temperature reaching -40°C.

According to the method recommended by the ISRM, all tested rocks had a core diameter of 50 mm, a surface parallel of ±0.1 mm, and a nominal length of 100 mm. In order to mimic the open-typed natural fractures and ensure that the effects of rock lithology are reduced on the experimental results, three preflaws were prepared using a water-jet system (Figure 2) within each cylindrical rock core. The mixture of high-pressure water with garnet abrasive from a 0.75 mm, 1.5 mm, and 2 mm diameter nozzle produced a defect with an aperture of 1 mm, 2 mm, and 3 mm, respectively. The geometric morphology of the treble-flaw sample is a combination of three horizontal flaws with a length of 12 mm, 24 mm, and 36 mm. For rock with the same lithology, the flaw width is set to be 1 mm, 2 mm, and 3 mm, respectively. To simulate the fill characteristics of natural fractures in the open pit slope, three fill types of no cementation, argillaceous cementation, and iron cementation were considered in this work.

2.2. Experimental Device and Method. After the preparation of preflawed samples, the rock samples were treated with vacuum saturation treatment for 24 hours with vacuum saturation apparatus (Figure 3) and then treated with freeze-thaw cycle. A specially self-developed frost heaving measurement system is used to monitor the evolution of frost heaving force, as shown in Figure 4. The system is composed of an ultralow temperature freezer, a film pressure sensor, a frost heaving force recording software, a date acquisition card, and a temperature-humility controller. The membrane pressure sensor is the core component of the system. Its model is the FSR402 made by Interlink Electronics. The size of the sensor is 5 mm in diameter and 38 mm in length. The sensor is a

rugged polymer thick film (PTF) device whose resistance decreases as the force applied to the sensor surface increases. The driving force is 0.2 N, the force sensitive range is 0.2 N~20 N, and the working temperature performance is cold -40°C with high temperature of 85°C. The recording frequency of the data acquisition system is 5 Hz, and the range of the temperature recorder is -200°C~80°C. It is equipped with a waterproof metal probe with the accuracy of ±0.2°C, and the data acquisition frequency is 1/60 Hz. According to the temperature change of the open pit slope, the saturated samples are put into the refrigerator unit and −30° C; then the samples are collected in the refrigerator and allowed to thaw. By doing so, a freeze-thaw cycle and frost heave force are achieved to monitor at the same time.

2.3. Testing Procedure. The detailed testing procedures are summarized as below:

(1) Firstly, the temperature of the digital control ultralow temperature refrigerator was set to be -30°C in advance, the waterproof treatment is carried out on the film sensor, and then its working state was checked again. The saturated rock samples with existing cracks were taken out from the vacuum saturator

(2) The frost heaving force test system was connected, and the temperature test system at the crack of the rock sample was installed. A syringe is then used to inject purified water into the crack and placed in the fridge while the monitoring system is activated. The frost heave force of three defects was tested in the same sample

(3) The evolution process of frost heaving force in F-T cycle was recorded. We continuously observe the FHF curve and measurement changes until the frost heaving force reaches the minimum value. The defective sample was then taken out of the ambient chamber and placed in air, and the FHF during the melting process was recorded at room temperature of 20°C until the frost heaving force reached zero

(4) The above experimental steps were repeated, and all samples were tested to obtain the frost heaving force evolution curves and also the peak FHF stress.

2.4. Frost Heaving Force Evolution Analysis. During a freeze-thaw cycle, typical FHF evolution curve is shown in Figure 5(a). FHF evolution for typical samples of sandstone, marble, and granite samples is shown in Figures 5(b)–5(d). It can be shown that five typical stages can be divided from the change of FHF; the evolution characteristic is described below:

(1) Inoculation stage of frost heaving force. At this stage, the temperature gradually drops below zero, but there is no frost heave force inside the crack. Although the temperature drops below zero, the water itself also stores a certain amount of heat, and at this stage, the defective water continues to give off heat until the temperature drops to about -5°C. When freezing occurs, the opening portion of the crack freezes first and then forms a frozen surface. The defect is in a closed system due to the ice jam effect. Although the volume expansion rate of water to ice is 9%, the frost heave force does not occur at this stage

(2) Sudden growth stage. With the decrease of temperature, the freezing degree of the sample increases, and the water-ice phase transition occurs constantly, which leads to the expansion of the volume in the crack. Due to the boundary limit of defect wall, the frost heave force of defect increases continuously. It can be seen from Figure 5(a) that the maximum frost heave force of cracks (granite, FW = 2 mm, FL = 24 mm, and no cementation) reaches 5.85 MPa

(3) Decline to steady stage. At this stage, the temperature continues to drop, but the frost heave force does not continue to increase. On the contrary, the frost heave force decreases and gradually stabilizes. This is because when the frost heaving force exceeds the

Table 2: Design of the Box-Behnken design table for frost heaving force measurement.

Run	A-FW (mm)	B-FL (mm)	C-CT (/)	D-RL (/)	FHF (MPa)
1	2	24	1	0	11.17
2	1	24	1	1	4.73
3	1	36	1	0	8.62
4	2	36	0	0	12.31
5	3	24	1	1	6.62
6	2	24	0	1	5.85
7	2	24	1	0	11.17
8	2	24	1	0	11.17
9	1	24	0	0	8.11
10	3	36	1	0	14.11
11	3	24	1	-1	5.01
12	2	12	1	1	7.45
13	2	12	0	0	5.08
14	2	24	2	1	13.32
15	2	12	1	-1	1.96
16	2	36	1	-1	2.67
17	2	36	1	1	13.77
18	2	36	2	0	15.62
19	1	24	2	0	10.34
20	3	24	2	0	16.08
21	3	24	0	0	13.72
22	2	24	1	0	11.17
23	1	12	1	0	9.31
24	2	24	0	-1	6.61
25	2	24	2	-1	7.68
26	2	12	2	0	12.37
27	3	12	1	0	12.07
28	2	24	1	0	11.17
29	1	24	1	-1	3.28

Table 3: Comparison of statistical models to choose the best RSM model for frost heaving force.

Source	Sum of squares	df	Mean square	F value	P value Prob > F	Fitness of the model
Mean vs. total	2620.291	1	2620.291			
Linear vs. mean	172.7944	4	43.1986	4.175242	0.0105	
2FI vs. linear	16.39158	6	2.731929	0.212032	0.9682	
Quadratic vs. 2FI	169.3645	4	42.34113	9.4758	0.0006	Suggested
Cubic vs. quadratic	47.08083	8	5.885104	2.281641	0.1653	Aliased
Residual	15.47598	6	2.579329			
Total	3041.398	29	104.8758			

Table 4: Statistical approach to select the RSM model for frost heaving force.

Source	Sum of squares	df	Mean square	F value	P value Prob > F	Significant
Model	358.5505	14	25.61075	5.731599	0.0012	Yes
A-FW	44.9307	1	44.9307	10.05534	0.0068	Yes
B-FL	29.64163	1	29.64163	6.633696	0.0220	Yes
C-CT	38.41341	1	38.41341	8.59679	0.0109	Yes
D-RL	59.80868	1	59.80868	13.38498	0.0026	Yes
AB	1.863225	1	1.863225	0.416983	0.5289	
AC	0.004225	1	0.004225	0.000946	0.9759	
AD	0.0064	1	0.0064	0.001432	0.9703	
BC	3.9601	1	3.9601	0.886257	0.3625	
BD	7.868025	1	7.868025	1.760837	0.2058	
CD	2.6896	1	2.6896	0.601923	0.4508	
A^2	3.588091	1	3.588091	0.803003	0.3853	
B^2	0.690416	1	0.690416	0.154513	0.7002	
C^2	15.23388	1	15.23388	3.40929	0.0861	
D^2	130.4771	1	130.4771	29.20034	<0.0001	
Residual	62.55681	14	4.468343			
Lack of fit	62.55681	10	6.255681			
Pure error	0	4	0			
Cor total	421.1073	28				

Table 5: Evaluation of different models to fit response value using statistical approach.

Source	Std. Dev.	R squared	Adjusted R squared	Predicted R squared	Press	Fitness of the model
Linear	3.216578	0.410333	0.312056	0.092253	382.259	
2FI	3.589501	0.449258	0.143291	-0.75435	738.7709	
Quadratic	2.113846	0.851447	0.702894	0.144334	360.3272	Suggested
Cubic	1.606029	0.963249	0.828497	-4.2921	2228.54	Aliased

tensile strength of the rock matrix, the crack tip is damaged, resulting in the dissipation of the frost heaving force. At this stage, new cracks appear at the crack tip and the rock structure deteriorates accordingly

(4) FHF recovery stage. When the frost heaving force reaches a steady state, the rock samples are taken out of the ultralow temperature refrigerator. The ice in the crack begins to melt, the frost heaving force increases with the increasing temperature, the second frost heaving occurs, and the curve of the frost heaving force shows the peak value. After the ice lens is formed, the frost heave force increases sharply in a short time. The crack tip damage results in the decrease of frost heave force. The second frost heave force is less than the first value, indicating that there is frost heave damage inside the crack

(5) Sudden drop stage. At this time, all the ice inside the crack melts and the frost heaving force caused by the secondary frost heaving dissipates gradually. Thus, the rock frost heave failure caused by frost heave force is terminated. The evolution process of frost heaving force is summarized, and it is found that the peak value of initial frost heaving force is the maximum strength that can be sustained when the crack is damaged. As a result, the initial peak value of frost heaving force can be used to characterize the frost heaving resistance of fractured rock mass.

3. Multiple Parameter Evaluation for Frost Heaving Force

3.1. Box-Behnken Design. To reveal the influence of geological discontinues on frost heaving force, in this work, four factors of flaw width, flaw length, flaw cement type, and rock lithology are investigated. Response surface method (RSM) is adopted to design the physical experiments, the studies' factors consider three levels, and the analysis step of this method is shown in Figure 6. Table 1 lists the considered factors that influences the frost heaving force. To the factor of cement type, coded method is used here, symbol of "0" indicates none filling, "1" indicates argillaceous cementation, and "2" indicates calcite cementation. To the factor of rock lithology, symbol of "-1" indicates sandstone, "0" indicates marble, and "1" indicates granite. By using the Box-Behnken design approach, a total of 29 runs are generated, including 5 repetitive cases, as listed in Table 2. As analyzed above, two peaks of FHF exist on the frost heaving force evolution curve, and the first peak value is larger than the second value. The peak FHF is a critical index to predict the fracturing of rock mass, and it is usually used to predict natural disasters related to freeze-thaw cycles. Here, the first peak frost heaving force is viewed as a response value, it is listed in the last column of Table 2.

3.2. RSM Model Analysis. As the experimental designed in Table 2, the RSM method is used to analyze the relationship between the response value and the four considered factors. In order to choose an appropriate RSM model, linear model, mean model, two-factor model interaction model (2FI), quadratic model, and cubic model are selected for judgment. According to the statistical method in Table 3, the best polynomial fitting equation is determined to predict the response values of FHF. Table 4 lists comparison of those selected models, and it shows that the P value of the quadratic function and 2FI function is less than 0.05, and the two models are suggested.

If the model has the highest polynomial, the other additional terms are significant, and the model is not aliased [31, 32], we select it as the appropriate model. If there is an alias, we will not select the cube model. Aliasing phenomenon reduces the number of experiments. When this occurs, the effects of several groups are combined into a single group, with the most significant effects in the group being used to represent the effects of the group. Essentially, it is important to note that the selected model should not have an alias characteristic. In order to further choose the best model, statistical approach is used, as shown in Table 5. It is also important to note that the selected model should have the maximum "predicted R squared" and "adjusted R squared" at the same time [33]. From the results of Table 5, the fully quadratic model is finally selected to build the maximum frost heaving force response surface in the subsequent optimization process.

Table 6: The optimal solutions to obtain the maximum frost heaving force considering the four factors.

Case	FW (mm)	FL (mm)	CT (/)	RL (/)	Peak FHF (MPa)	Desirability
1	2.17	35.93	1.96	0.55	16.0968	1
2	2.91	24.26	2	0.37	16.2271	1
3	2.93	25.66	1.98	0.14	16.1325	1
4	2.56	32.09	1.88	0.57	16.1639	1
5	2.71	33.3	2	0.56	17.0619	1
6	3	24.37	1.98	0.43	16.1486	1
7	2.6	32.47	1.88	0.35	16.307	1
8	2.85	30.01	1.88	0.43	16.3856	1
9	3	34.99	1.78	0.1	16.1632	1
10	2.71	31	1.86	0.31	16.1921	1
11	2.96	34.49	1.74	0.31	16.4357	1
12	2.91	27.49	1.99	0.22	16.5089	1
13	2.99	33.58	1.93	0.04	16.3928	1
14	2.83	24.61	2	0.2	16.0967	1
15	2.79	31.25	1.96	0.04	16.096	1
16	2.5	33.86	1.93	0.68	16.3282	1
17	2.39	34.77	1.93	0.36	16.3462	1
18	2.96	27.92	1.98	0.29	16.6224	1
19	2.5	34.56	1.89	0.51	16.416	1
20	2.65	34.56	1.98	0.39	16.999	1

Using the ANOVA analysis, the response value of FHF obtained by the quadratic model is listed in Table 6. The result shows that the model F value is 5.73 m implying that the model is very significant. The change of P value is 0.2% less than that of a "model F value," this large value could occur due to noise. The variations of the four considered factors are all significant as the "Prob > F" is less than 0.05 for the quadratic model. In this case, the model P value of the studied factors is <0.0068, 0.022, 0.0109, and 0.0026, indicating that the considered factors of flaw width, flaw length, cementation, and rock lithology are all significant model terms. The smaller the P value pro, the more sensitive the factor is to the response surface. The influential order of the four factors is D-rock lithology > A-flaw width > C-Cement type > B-flaw length. The final equations for the frost heaving force in terms of actual factors are

$$\begin{aligned} FHF = {} & +0.4250 + 3.5125A + 0.20889B + 0.64917C \\ & - 1.4725D + 0.0569AB + 0.0325A \times C + 0.04A \times D \\ & - 0.8325B \times C + 0.11687B \times D + 0.85C \times D \\ & - 0.7437A2 + 1.532C^2 - 4.485D^2. \end{aligned} \quad (1)$$

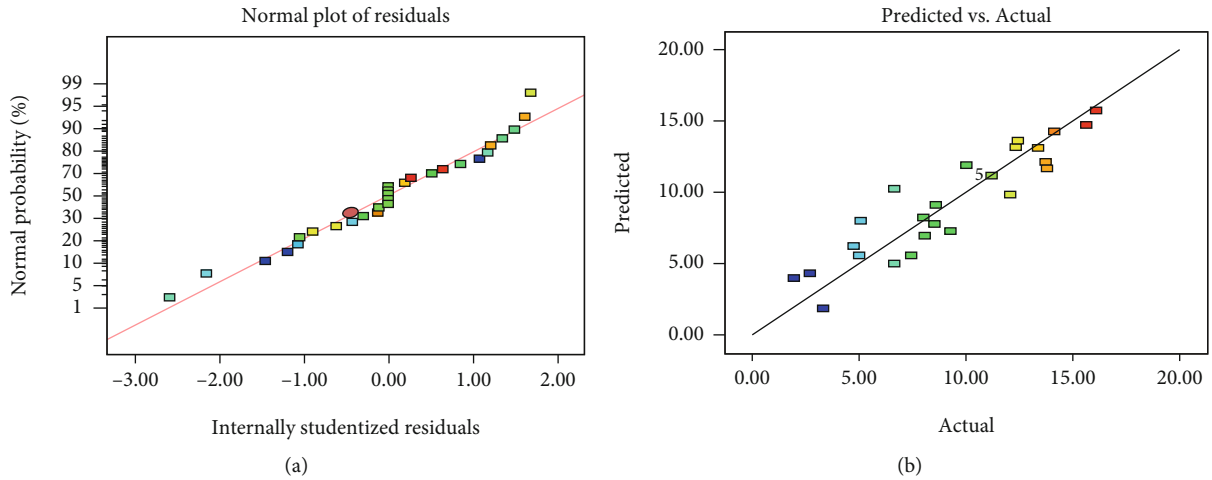

Figure 7: Illustration of the reliability of the response model to the frost heaving force. (a) Internally studentized residual distribution for the FHF value. (b) Comparison of the predicted FHF and the actual FHF.

In order to reflect the reliability of the response model to fit the FHF, Figure 7(a) plots the relationship between the studentized residuals and the normal probability. It can be seen that all the testing points in the "Normal Plot of Residuals" are along the straight line. This result indicates that the residuals are normally distributed, and the model is significant accordingly. To illustrate whether the generated equation of the gradient response surface accurately predicts the actual values, Figure 7(b) shows the difference between the predicted value and the actual measurement value for frost heaving force. The predicted FHF and actual FHF distribute evenly at both sides of the "Predicted versus Actual" curve, implying that generated frost heaving force gradient response surface models provide such reliable predicted values for frost heaving force.

After fitting of the FHF using the quadratic function, all the experimental design results are generated using RSM analysis. Figure 8 shows the 3D response surface and 2D response contour for the four considered factors, and the response surface represents all the 29 run cases in Table 2. The influential trend of FW, FL, CT, and RL to FHF can be observed from the response surface. Figure 8(a) plots the impact of the factor flaw width and flaw length on frost heaving force. It can be seen that frost heaving force increases with increasing flaw width and flaw length, and the impact of flaw width is much obvious than flaw length. With the increases of flaw width and length, the volume of ice increases, and frost heaving force resulting from the expansion of water-ice transformation increases with increasing flaw volume. Figure 8(b) plots the impact of the factor flaw width and cement type on frost heaving force. It shows that strong cement characteristics of the flaws would result in the generation of high frost heaving force. Figure 8(c) plots the impact of the factor flaw width and rock lithology on frost heaving force. Nonlinear changes can be observed from the results, for rock lithology changes from sandstone to granite, frost heaving force first increases, and then decreases. The impact of rock lithology on frost heaving force is complex, other factors should be introduced at the same time. This result reflects that water migration into the rock matrix is closely related to rock lithology, and the associated mesoscopic structure of rock influences the damage propagation caused by the frost heaving force. As shown in Figure 8(d), the impact of cement type and rock lithology on frost heaving force is studied. Similar result can be drawn that frost heaving force becomes larger for flaw with strong cementation. The effect of rock lithology on frost heaving force evolution presents complex pattern, and this is attributed to the water migration ability depending on the mesoscopic structure of rock matrix.

3.3. Maximum Frost Heaving Force Prediction. The maximum frost heaving force (FHF) is impacted by flaw geometric parameter and also the rock physical properties. The higher the FHF, the higher the rock structural deterioration degree is. Rock failure owing to frost heaving impacts the stability of rock constructions; therefore, predicting the maximum frost heaving force is crucial in cold regions. The RSM numerical optimization algorithm is used to find the variable set of the four factors resulting in the maximum FHF value. Through RSM numerical optimization, a total of 55 optimal solutions were obtained. The desired value is between 0.842 and 1.00. We choose the solution with the maximum expected value for analysis. Figure 9 shows the relationship between the studied factors and the desirability values. From the optimization result, it shows that the buildup of frost heaving force with flaws is impacted by multiple factors, and those factors interact to determine the value of frost heaving force. When the desirability value equals to 1, the crack width and length are not the largest, it is shown that a smaller width usually matches with a short length, and a larger width matches with a smaller length. This is to say, the frost heaving force is simultaneous determined by the width and length. As shown in Figure 9, it shows that strong cementation could lead to relatively larger frost heaving force. The iron cementation characteristic filled into the flaw results in relatively large frost heaving force. The optimization result of rock lithology shows that

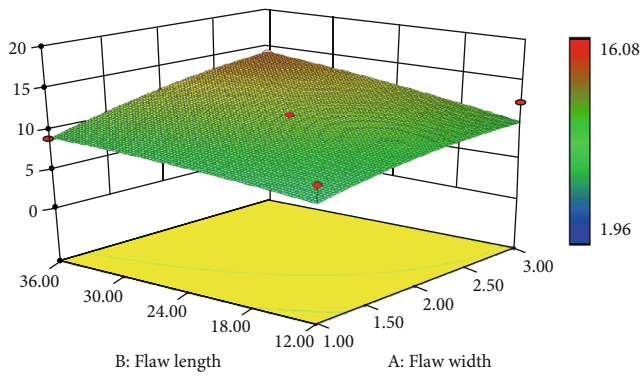

Actual factors:
B: Cement type = 1.00
C: Rock lithology = 0.00

X1 = A: Flaw width
X2 = B: Flaw length

(a)

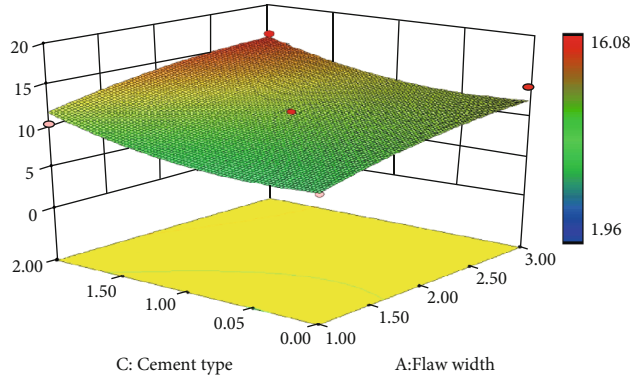

Actual factors:
B: Flaw length = 24.00
D: Rock lithology = 0.00

X1 = A: Flaw width
X2 = C: Cement type

(b)

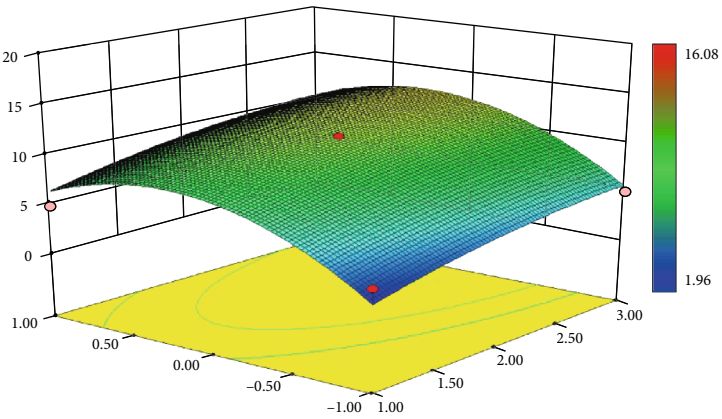

Actual factors:
B : Flaw length = 24.00
C : Cemnet type = 1.00

X1 = A : Flaw width
X2 = D : Rock lithology

(c)

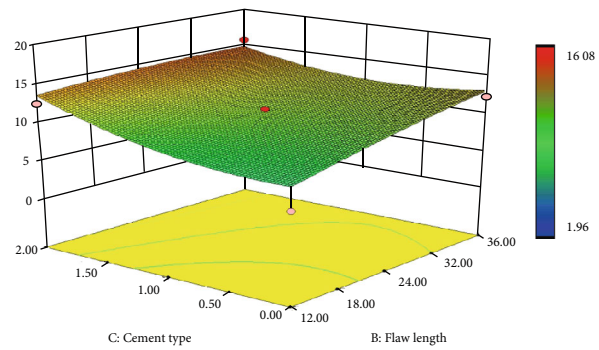

Actual factors:
A: Flaw width = 2.00
D: Rock lithology = 0.00

X1 = B: Flaw length
X2 = C: Cement type

(d)

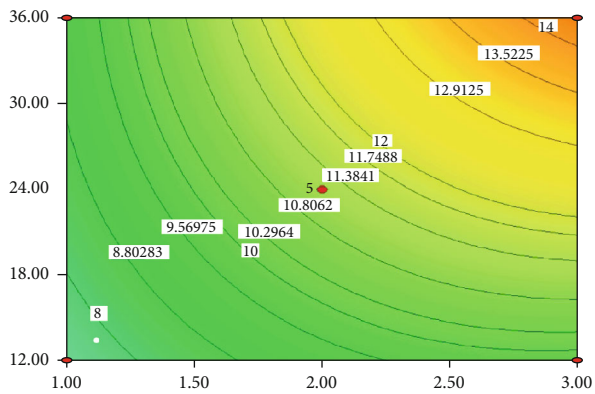

Actual factors:
B: Cement type = 1.00
C: Rock lithology = 0.00

X1 = A: Flaw width
X2 = B: Flaw length

(e)

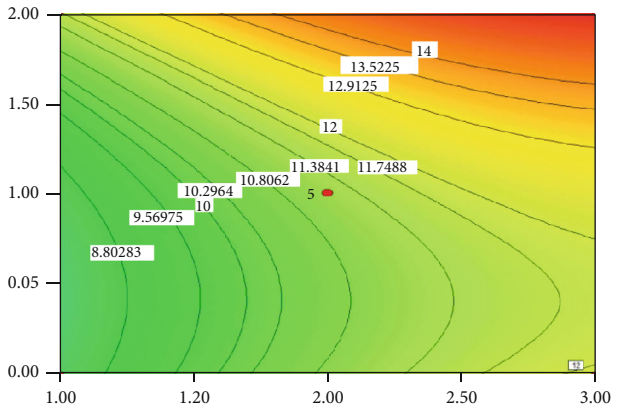

Actual factors:
B: Flaw length = 24.00
D: Rock lithology = 0.00

X1 = A: Flaw width
X2 = C: Cement type

(f)

Figure 8: Continued.

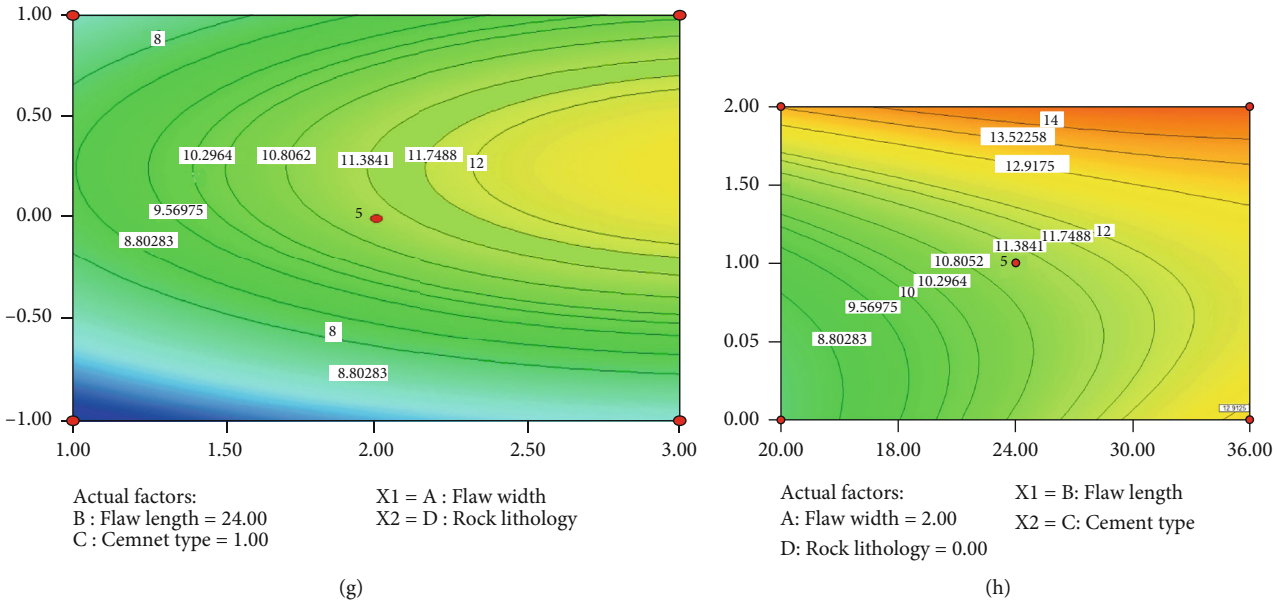

Figure 8: Response of the influential factors on frost heaving force. (a–d) 3D response surface analysis of the influence of the four factors on frost heaving force. (e–h) 2D contour of the influence of the four factor on frost heaving force.

the granite samples are prone to generate high frost heaving force. Among the 55 optimal solutions, Table 6 lists the top 20 combinations to predict frost heaving force when the desirability is 1.

3.4. Discussions. In cold regions, especially the high-altitude cold region, the rock mass is always subjected to cyclic freeze-thaw weathering. Under freeze conditions, the frost heaving force with rock discontinuity would accelerate the damage of rock structure and result in the stability of rock mass. The measurement of frost heaving force is necessary to evaluate and predict the rock deterioration degree. Several studies were performed to measure the frost heaving force within rock cracks, and most of the investigations are focused on a single factor [18, 21–23]; the multiple factors impacting the evolution of frost heaving force are not well understood. For the four factors studied in this work, it shows that the flaw width is the most sensitive factor to frost heaving force, and flaw length is the least sensitive factor. Frost heaving force is actually a kind of tensile stress; fracturing occurs if the frost heaving exceeds rock tensile strength [34]. Vertical to the crack propagation path, the increasing flaw width is prone to lead to flaw damage and degradation. When the crack presents as cement state, the filled material has different responses to water migration and water-ice transformation, and this would result in the difference of frost heaving force accumulation and releases. The testing results show that strong cement material can lead to relatively high frost heaving force, vice versa. Rock lithology is a determining factor influencing the evolution of frost heaving forces. Previous studies show that rock porosity and strength characteristics influence the frost heaving process [35]. For soft rock, altered rock, or high-porosity rocks, during water-ice transformation, water seepages flow into micropores, and freezing leads to the occurrence of the expansion of pore water crystal; internal frost heave pressure occurs in pores, and the porosity gradually increases after freezing. However, for hard rock with low porosity and relatively high strength, the existence of microcracks contributes a lot to frost heaving. During water-ice transformation, moisture penetrates into the defects, ice lens forms, and frost heaving appears on the defect surface; the ice lens grows as water continuously penetrates into the defects. In this work, the sandstone is a typical high-porosity rock, and the pores have obvious influence on frost heaving. For marble, the water is hard to penetrate into rock matrix, ice lens is difficult to form during freezing process, and rock damage degree is the least. However, for the granite, it is a kind of medium-low grain rock, microcracks exist at the mineral interfaces, water is easily penetrated into rock matrix compared to marble, and a lot of ice lens forms. As proved by other studies that the mesoscopic structural characteristics of rock control its macroscopic mechanical responses [33, 36–41], this work further proves this finding. The basic reason causing the difference of frost heaving force evolution is the mesoscopic structures. The testing results also indicate that the frost heaving force is relatively small for sandstone than marble and granite. In this work, artificially prepared flaws were used to measure frost heaving force; in the further studies, frost heaving measurement should be done within the original cracks; in addition, the frost heaving force after multiple freeze-thaw cycles should be studied; moreover, the freeze-thaw loading is a kind of fatigue loading, and cyclic F-T would have strong effect on the determination of rock structure and its stability. Although the cyclic mechanical behaviors of rock subjected to mechanical loading have been widely [42–45], the investigations about the coupling F-T and mechanical loads on rock geomechanical behaviors are not well understood and should be deeply investigated in the further studies.

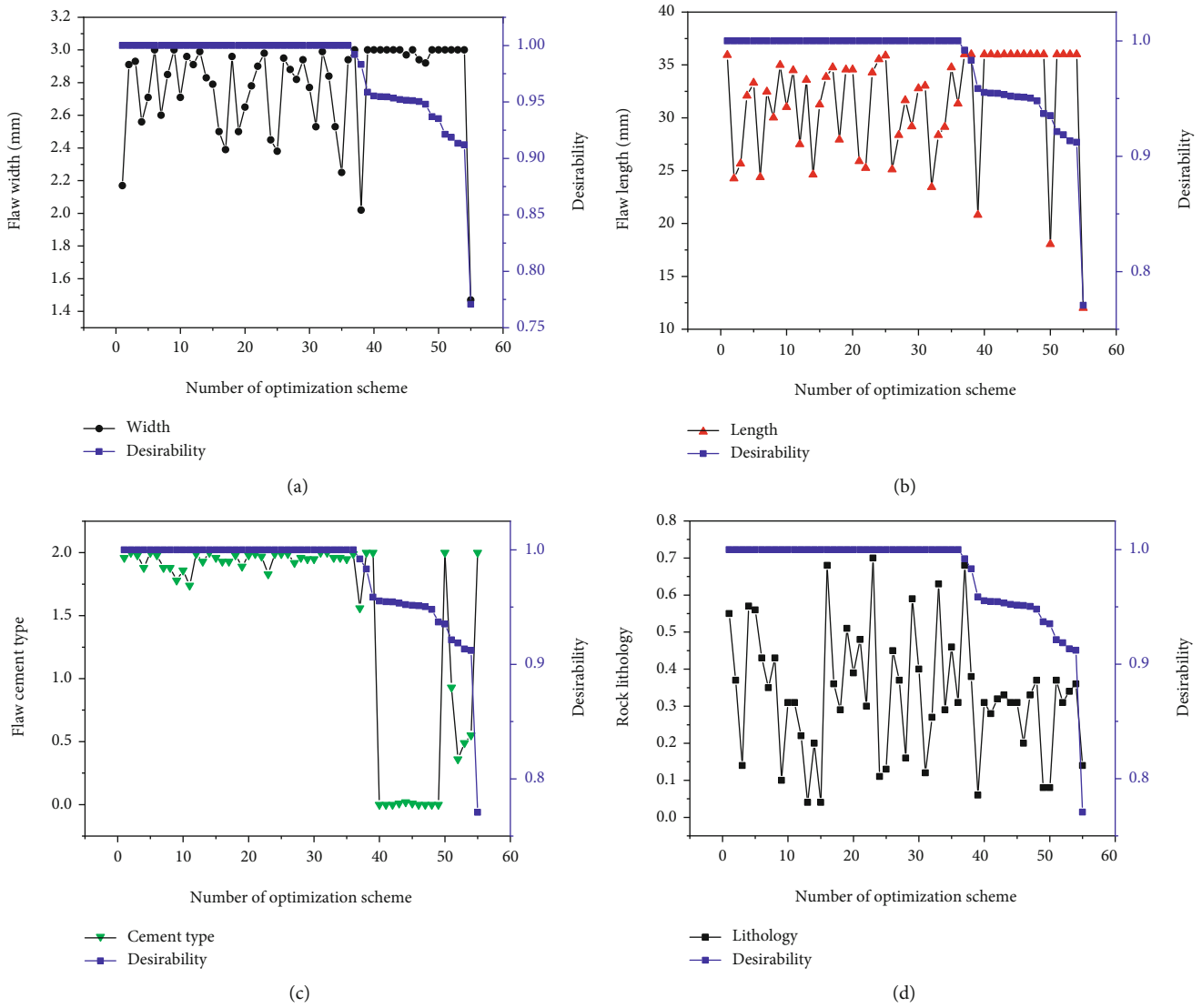

Figure 9: Optimal combinations to maximize the frost heaving force. (a–d) Plots of the optimal factors of flaw width, flaw length, flaw cement type, and rock lithology, respectively.

4. Conclusions

This paper conducts real-time frost heaving force measurement for different rocks with various flaw geometric shape and cementation type. A specially designed frost heaving force measurement system is employed to monitor the evolution of frost heaving force. Main conclusions can be summarized below:

(1) Multistage frost heaving force evolution is observed, and the peak frost heaving force occurs twice during a freeze-thaw cycle. After formation of ice lens, frost heaving force sharply increases within a short time. Damage in the flaw tips leads to the decreasing of frost heaving force. The secondary frost heaving force is less than the first value, indicating that frost heaving damage occurs within the cracks

(2) By the RSM evaluation, the influential order of the studied factors to frost heaving degradation is firstly obtained; rock lithology is the most sensitive factor to the maximum frost heaving force. The influential order is rock lithology > flaw width > flaw cement type > flaw length

(3) It is not the case that the larger the ice lens volume, the larger the frost heaving force. The influence of flaw width and length to the maximum frost heaving force is not independent but interactive. Rock lithology determines the water migration ability and influences the water-ice phase transformation

(4) For low-pore hard rock, increasing flaw width, flaw length, and flaw cement strength can improve the possibility to frost heaving failure. For rock mass construction in cold regions, the rock mass subjected to low-stress disturbance would decrease the crack

scale, and this could sustain the long-term stability of rock mass.

Data Availability

The experimental data used to support the findings of this study are included within the article.

Conflicts of Interest

The authors declare no conflict of interest.

Acknowledgments

The authors would like to thank the editors and the anonymous reviewers for their helpful and constructive comments. This research was funded by the National Key Technologies Research and Development Program (2018YFC0808402), the Beijing Natural Science Foundation (8202033), and the Fundamental Research Funds for the Central Universities (FRF-TP-20-004A2).

References

[1] N. Matsuoka, "Microgelivation versus macrogelivation: towards bridging the gap between laboratory and field frost weathering," *Permafrost Periglac*, vol. 12, no. 3, pp. 299–313, 2001.

[2] Y. Wang, S. H. Gao, C. H. Li, and J. Q. Han, "Investigation on fracture behaviors and damage evolution modeling of freeze-thawed marble subjected to increasing- amplitude cyclic loads," *Theoretical and Applied Fracture Mechanics*, vol. 109, article 102679, 2020.

[3] M. Takarli, W. Prince, and R. Siddique, "Damage in granite under heating/cooling cycles and water freeze-thaw condition," *International Journal of Rock Mechanics and Mining Sciences*, vol. 45, no. 7, pp. 1164–1175, 2008.

[4] X. J. Tan, W. Z. Chen, J. P. Yang, and J. J. Cao, "Laboratory investigations on the mechanical properties degradation of granite under freeze-thaw cycles," *Cold Regions Science and Technology*, vol. 68, no. 3, pp. 130–138, 2011.

[5] Y. Wang and C. H. Li, "Investigation on crack coalescence behaviors for granite containing two flaws induced by cyclic freeze-thaw and uniaxial deformation in Beizhan Iron Mining, Xinjing, China," *Geofluids*, vol. 2020, 19 pages, 2020.

[6] S. Gruber and W. Haeberli, "Permafrost in steep bedrock slopes and its temperature-related destabilization following climate change," *Journal of Geophysical Research - Earth Surface*, vol. 112, pp. 148–227, 2007.

[7] Y. Wang, W. K. Feng, H. J. Wang, C. H. Li, and Z. Q. Hou, "Rock bridge fracturing characteristics in granite induced by freeze-thaw and uniaxial deformation revealed by AE monitoring and post-test CT scanning," *Cold Regions Science and Technology*, vol. 177, article 103115, 2020.

[8] Y. Wang, X. F. Yi, S. H. Gao, and H. Liu, "Laboratory Investigation on the Effects of Natural Fracture on Fracture Evolution of Granite Exposed to Freeze-Thaw-Cyclic (FTC) Loads," *Geofluids*, pp. 1–20, 2021.

[9] S. Weber, J. Beutel, J. Faillettaz, A. Hasler, M. Krautblatter, and A. Vieli, "Quantifying irreversible movement in steep, fractured bedrock permafrost on Matterhorn (CH)," *The Cryosphere*, vol. 11, no. 1, pp. 567–583, 2017.

[10] F. Musso Piantelli, M. Herwegh, F. S. Anselmetti, M. Waldvogel, and U. Gruner, "Microfracture propagation in gneiss through frost wedging: insights from an experimental study," *Natural Hazards*, vol. 100, no. 2, pp. 843–860, 2020.

[11] T. C. Hales and J. J. Roering, "Climatic controls on frost cracking and implications for the evolution of bedrock landscapes," *Journal of Geophysical Research - Earth Surface*, vol. 112, pp. 315–328, 2007.

[12] B. Hallet, J. S. Walder, and C. W. Stubbs, "Weathering by segregation ice growth in microcracks at sustained subzero temperatures: verification from an experimental study using acoustic emissions," *Permafrost Periglac Process*, vol. 2, no. 4, pp. 283–300, 1991.

[13] K. Hall and C. Thorn, "The historical legacy of spatial scales in freeze–thaw weathering: misrepresentation and resulting misdirection," *Geomorphology*, vol. 130, no. 1-2, pp. 83–90, 2011.

[14] B. Hallet, "Geology: why do freezing rocks break?," *Science*, vol. 314, no. 5802, pp. 1092-1093, 2006.

[15] M. G. Worster and J. S. Wettlaufer, "The fluid mechanics of premelted liquid films," in *Fluid dynamics at interfaces*, W. Shyy and R. Narayanan, Eds., pp. 339–351, Cambridge University Press, Cambridge, 1999.

[16] H. Jia, K. Leith, and M. Krautblatter, "Path-dependent frost-wedging experiments in fractured, low-permeability granite," *Permafrost Periglac Process*, vol. 28, no. 4, pp. 698–709, 2017.

[17] M. Ishikawa, Y. Kurashige, and K. Hirakawa, "Analysis of crack movements observed in an alpine bedrock cliff," *Earth Surface Processes and Landforms*, vol. 29, no. 7, pp. 883–891, 2004.

[18] E. M. Winkler, "Frost damage to stone and concrete: geological considerations," *Engineering Geology*, vol. 5, no. 2, pp. 315–323, 1968.

[19] G. Bai, D. Gao, Z. Liu, X. Zhou, and J. Wang, "Probing the critical nucleus size for ice formation with graphene oxide nanosheets," *Nature*, vol. 576, no. 7787, pp. 437–441, 2019.

[20] S. Akagawa and M. Fukuda, "Frost heave mechanism in welded tuff," *Permafrost and Periglacial Processes*, vol. 2, no. 4, pp. 301–309, 1991.

[21] D. Arosio, L. Longoni, and F. Mazza, "Freeze-thaw cycle and rockfall monitoring," in *Landslide Science and Practice*, pp. 385–390, Springer Verlag, Berlin, 2013.

[22] G. P. Davidson and J. F. Nye, "A photoelastic study of ice pressure in rock cracks," *Cold Regions Science and Technology*, vol. 11, no. 2, pp. 141–153, 1985.

[23] S. B. Huang, Q. S. Liu, and A. P. Cheng, "Preliminary experimental study of frost heaving pressure in crack and frost heaving propagation in rock mass under low temperature," *Rock and Soil Mechanics*, vol. 39, no. 1, pp. 78–84, 2018.

[24] Y. Wang, S. H. Gao, C. H. Li, and J. Q. Han, "Energy dissipation and damage evolution for dynamic fracture of marble subjected to freeze-thaw and multiple level compressive fatigue loading," *International Journal of Fatigue*, vol. 142, article 105927, 2021.

[25] C. Xia, Z. Lv, Q. Li, J. Huang, and X. Bai, "Transversely isotropic frost heave of saturated rock under unidirectional freezing condition and induced frost heaving force in cold region tunnels," *Cold Regions Science and Technology*, vol. 152, no. 152, pp. 48–58, 2018.

[26] J. P. McGreevy and W. B. Whalley, "Rock moisture content and frost weathering under natural and experimental conditions: a comparative discussion," *Arctic and Alpine Research*, vol. 12, no. 6, pp. 337–346, 1985.

[27] S. Huang, Q. Liu, Y. Liu, Y. Kang, A. Cheng, and Z. Ye, "Frost heaving and frost cracking of elliptical cavities (fractures) in low- permeability rock," *Engineering Geology*, vol. 234, pp. 1–10, 2018.

[28] H. Liu, X. Yuan, and T. Xie, "A damage model for frost heaving pressure in circular rock tunnel under freezing-thawing cycles," *Tunnelling and Underground Space Technology*, vol. 83, pp. 401–408, 2019.

[29] Q. S. Liu, S. B. Huang, Y. S. Kang, Y. C. Pan, and X. Z. Cui, "Experimental and theoretical studies on frost heaving pressure in a single fracture of frozen rock mass under low temperature," *Chinese Journal of Geotechnical Engineering*, vol. 37, no. 9, pp. 1572–1580, 2015, (In Chinese).

[30] Z. Lv, C. Xia, Y. Wang, and J. Luo, "Analytical elasto-plastic solution of frost heaving force in cold region tunnels considering transversely isotropic frost heave of surrounding rock," *Cold Regions Science and Technology*, vol. 163, pp. 87–97, 2019.

[31] Y. Wang, C. Li, X. Zhou, and X. Wei, "Seepage piping evolution characteristics in bimsoils—an experimental study," *Water*, vol. 9, no. 7, p. 458, 2017.

[32] Y. Wang, X. Li, R. Hu, C. F. Ma, Z. Z. Zhao, and B. Zhang, "Numerical evaluation and optimization of multiple hydraulically fractured parameters using a flow-stress-damage coupled approach," *Energies*, vol. 325, no. 9, 2016.

[33] C. Zhu, M. C. He, M. Karakus, X. B. Cui, and Z. G. Tao, "Investigating toppling failure mechanism of anti-dip layered slope due to excavation by physical modeling," *Rock Mechanics and Rock Engineering*, vol. 53, no. 11, pp. 5029–5050, 2020.

[34] N. Matsuoka and J. Murton, "Frost weathering: recent advances and future directions," *Permafrost and Periglacial Processes*, vol. 19, no. 2, pp. 195–210, 2008.

[35] X. Luo, N. Jiang, C. Zuo, Z. Dai, and S. Yan, "Damage characteristics of altered and unaltered diabases subjected to extremely cold freeze–thaw cycles," *Rock Mechanics and Rock Engineering*, vol. 47, no. 6, pp. 1997–2004, 2014.

[36] D. K. Liu, Z. L. Gu, R. X. Liang et al., "Impacts of pore-throat system on fractal characterization of tight sandstones," *Geofluids*, vol. 2020, 17 pages, 2020.

[37] Y. Wang, W. K. Feng, R. L. Hu, and C. H. Li, "Fracture evolution and energy characteristics during marble failure under triaxial fatigue cyclic and confining pressure unloading (FC-CPU) conditions," *Rock Mechanics and Rock Engineering*, vol. 34, pp. 1–20, 2020.

[38] Z. Li, S. Liu, W. Ren, J. Fang, Q. Zhu, and Z. Dun, "Multiscale laboratory study and numerical analysis of water-weakening effect on shale," *Advances in Materials Science and Engineering*, vol. 2020, Article ID 5263431, 2020.

[39] Q. Meng, H. Wang, M. Cai, W. Xu, X. Zhuang, and T. Rabczuk, "Three-dimensional mesoscale computational modeling of soil-rock mixtures with concave particles," *Engineering Geology*, vol. 277, article 105802, 2020.

[40] Y. Wang, W. K. Feng, and C. H. Li, "On anisotropic fracture and energy evolution of marble subjected to triaxial fatigue cyclic-confining pressure unloading conditions," *International Journal of Fatigue*, vol. 134, article 105524, 2020.

[41] J. Wang, Y. Zhang, Z. Qin, S. G. Song, and P. Lin, "Analysis method of water inrush for tunnels with damaged water-resisting rock mass based on finite element method-smooth particle hydrodynamics coupling," *Computers and Geotechnics*, vol. 126, article 103725, 2020.

[42] Y. Wang, S. Gao, D. Liu, and C. H. Li, "Anisotropic fatigue behaviour of interbeded marble subjected to uniaxial cyclic compressive loads," *Fatigue & Fracture of Engineering Materials & Structures*, vol. 43, no. 6, pp. 1170–1183, 2020.

[43] Y. Wang, D. Liu, J. Han, C. Li, and H. Liu, "Effect of fatigue loading-confining stress unloading rate on marble mechanical behaviors: an insight into fracture evolution analyses," *Journal of Rock Mechanics and Geotechnical Engineering*, vol. 12, no. 6, pp. 1249–1262, 2020.

[44] Y. Wang, C. H. Li, and J. Q. Han, "On the effect of stress amplitude on fracture and energy evolution of pre-flawed granite under uniaxial increasing-amplitude fatigue loads," *Engineering Fracture Mechanics*, vol. 240, article 107366, 2020.

[45] Y. Wang, C. Li, J. Han, and H. Wang, "Mechanical behaviours of granite containing two flaws under uniaxial increasing amplitude fatigue loading conditions: an insight into fracture evolution analyses," *Fatigue & Fracture of Engineering Materials & Structures*, vol. 224, pp. 1–16, 2020.